# $InCrBr_3$: A Ternary Indium Bromide Containing Jahn−Teller Unstable $Cr^{2+}$ and the Magnetic Structures of $InCrBr_3$ and $InFeBr_3$

**Michael Scholten and Richard Dronskowski***

Institut für Anorganische Chemie, Rheinisch−Westfälische Technische Hochschule Aachen, Prof.-Pirlet-Strasse 1, 52 074 Aachen, Germany

**Herbert Jacobs**

Fachbereich Chemie, Universität Dortmund, Otto-Hahn-Strasse 6, 44 221 Dortmund, Germany

*Received December 3, 1998*

Yellow needles of $InCrBr_3$ are synthesized from molten $InBr_3$ and elemental Cr at 450 °C. Its monoclinic crystal structure ($a = 412.09(3)$ pm, $b = 1500.6(1)$ pm, $c = 937.65(6)$ pm, $\beta = 94.386(6)°$; $P2_1/c$; $Z = 4$), similar to the $NH_4CdCl_3$ type, has been determined by single crystal structure investigations. While the chromium cations are found in Jahn−Teller distorted $Br^-$ octahedra, monovalent indium cations are located in strongly distorted trigonal $Br^-$ prisms which are tricapped by additional $Br^-$ anions. $InCrBr_3$ shows Curie−Weiss paramagnetism and exhibits antiferromagnetic ordering below 12 K. Ab initio band structure calculations reveal that the indium−bromine bonds are weakened due to out-of-phase interactions in the highest occupied bands. Neutron diffraction experiments at 2 K for $InCrBr_3$ and $InFeBr_3$ yield additional reflections because of antiferromagnetic ordering. Both spin structures have been determined and refined on the basis of the Rietveld method.

## 1. Introduction

Recent years have seen considerable progress in the synthesis and characterization of binary and ternary bromides containing low valent indium (refs 1 and 2 and references cited within). In all of these compounds, the antibonding interactions of the $In^+$ cation with bromine anions[3] lead both to uncommon, often distorted coordination polyhedra and to enhanced reactivities in their melts (with transition metals) or even in the solid state (with organic molecules). Within the group of ternary indium bromides, $InFeBr_3$, $InMnBr_3$, $InCdBr_3$, and $InMgBr_3$ adopt the $NH_4CdCl_3$ structure type. By using chromium we intended to introduce a Jahn−Teller unstable ion into this structure type. Since divalent chromium has a $d^4$ configuration, a weak octahedral field might induce a Jahn−Teller distortion. In the following we report on the synthesis, crystal structure, chemical bonding, and magnetic properties of the new ternary phase $InCrBr_3$ and, in addition, on the magnetic structures of $InCrBr_3$ and $InFeBr_3$.

## 2. Experimental and Theoretical Techniques

**2.1. Synthesis.** $InCrBr_3$ and $InFeBr_3$ were synthesized by heating equimolar amounts of indium tribromide (prepared from aqueous solution and purified by repeated sublimation[4]) and chromium or iron metal powder (Alfa Products, purity 99.95% and 99.9%, used as purchased) within an evacuated glass ampule at 450 °C for 5 days. The melt was slowly cooled down to 100 °C at a rate of 2 °C/h, then to room temperature at 20 °C/h. $InCrBr_3$ and $InFeBr_3$ crystallize as yellow transparent needles. Also, $InCrBr_3$ and $InFeBr_3$ are extremely sensitive to air and humidity and must be strictly handled under a protective argon atmosphere.

**2.2. Structure Determination. 2.2.1. Crystal Structure of $InCrBr_3$.** A fast Guinier−Simon[5] powder photograph showed the presence of the monoclinic crystal system. Since $InCrBr_3$ decays when exposed to Cu $K\alpha_1$ radiation, it was impossible to collect any useful intensity data on a powder diffractometer. The monoclinic symmetry was confirmed using a single crystal ($0.11 \times 0.06 \times 0.14$ mm$^3$) mounted on an imaging plate diffractometer (Stoe IPDS, Mo K$\alpha$ radiation, graphite monochromator). After having collected a complete data set (max 50° in 2$\Theta$; $-5 \le h \le 5$, $0 \le k \le 21$, $0 \le l \le 13$; 7221 reflections of which 1554 were independent with $R_{merge} = 0.041$), the absorption correction was performed numerically (indexed faces: (100) ↔ ($\bar{1}$00) (long), (010) ↔ (0$\bar{1}$0) (middle), (001) ↔ (00$\bar{1}$) (short)) and the range of the calculated transmission was between 0.083 and 0.216. The systematic absences unambiguously indicated space group $P2_1/c$-$C_{2h}^5$ (no. 14), and both structure solution (Direct Methods, SHELXS-86[6]) and structure refinement (SHELX-76[7]) were straightforward using the scattering factors of the neutral atoms.[8] After allowing anisotropic displacement parameters in the refinement, the $R_w$ residual came to 0.078; the lattice parameters were refined from a fast powder data scan where intensity errors are unimportant. Corrections for the presence of extinction had no influence on the quality of the refinement.

For all atoms, the components of the anisotropic displacement factors are very well behaved. It is obvious, however, that the isotropic displacement factor of In is about 20% larger than those of the other atoms. This characteristic effect for an $In^+$ position is due to the very soft $In^+$−$Br^-$ crystal potential and not because of a possible suboccupation of the indium site.

The final difference Fourier map was flat, and the strongest residual peak was about 135 pm apart from the In position. Table 1 shows all relevant data of the structure analysis while Table 2 contains positional

(1) Dronskowski, R. *Angew. Chem., Int. Ed. Engl.* **1995**, *34*, 1126.
(2) Dronskowski, R. *Z. Kristallogr.* **1995**, *210*, 920.
(3) Dronskowski, R. *Inorg. Chem.* **1994**, *33*, 6201.
(4) Ensslin, F.; Dreyer, H. *Z. Anorg. Allg. Chem.* **1942**, *249*, 119.
(5) Simon, A. *J. Appl. Crystallogr.* **1970**, *3*, 18.
(6) Sheldrick, G. M. *SHELXS-86, Program for Crystal Structure Determination*; Universität Göttingen: Göttingen, Germany, 1986.
(7) Sheldrick, G. M. *SHELX-76, Program for Crystal Structure Determination*; Universität Göttingen: Göttingen, Germany, 1976.
(8) *International Tables for Crystallography, Volume C*; Wilson, A. J. C., Ed.; Kluwer Academic Publishers: Dordrecht, 1992.

10.1021/ic981383t CCC: $18.00 
Published on Web 05/01/1999

**Table 1.** Crystallographic Data for $InCrBr_3$

| | |
|---|---|
| chemical formula $InCrBr_3$ | formula weight 406.53 g/mol |
| $a = 412.09(3)$ pm | space group $P2_1/c$ (no. 14) |
| $b = 1500.6(1)$ pm | $\lambda = 71.073$ pm |
| $c = 937.65(6)$ pm | $\rho_{calcd} = 4.667$ g/cm$^3$ |
| $\beta = 94.386(6)°$ | $\mu = 26.42$ mm$-1$ |
| $V = 578.1 \times 10^6$ pm$^3$ | $R(F_o \geq 3\sigma(F_o))^a = 0.069$ |
| $Z = 4$ | $R_w{}^b = 0.078$ |
| $T = 20(1)$ °C | |

[a] $R = \sum|F_o - |F_c||/\sum(F_o)$. [b] $R_w = \sum w(F_o - |F_c|)^2/\sum wF_o{}^2$.

**Table 2.** Positional Parameters (All Atoms on Wyckoff Position 4*e*) and Isotropic Displacement Parameters ($U_{iso}$ in pm$^2$) for $InCrBr_3$ (Standard Deviations in Parentheses)

| atom | *x* | *y* | *z* | $U_{iso}$ |
|---|---|---|---|---|
| In | 0.7627(5) | 0.1712(2) | 0.0477(2) | 414(8) |
| Cr | 0.2375(9) | 0.4487(2) | 0.1586(4) | 201(12) |
| Br(1) | 0.2068(5) | 0.6013(2) | 0.0330(2) | 205(8) |
| Br(2) | 0.7081(6) | 0.5050(2) | 0.3276(2) | 233(8) |
| Br(3) | 0.2634(6) | 0.2959(2) | 0.2711(3) | 277(9) |

**Table 3.** Selected Interatomic Distances (pm) in $InCrBr_3$ (Standard Deviations in Parentheses)[a]

| | | | |
|---|---|---|---|
| In−Br(3g) | 322.3(3) | In−In(a) | 412.1(3) |
| In−Br(2g) | 335.1(3) | In−In(b) | 412.1(3) |
| In−Br(3a) | 338.9(3) | In−Cr | 432.8(4) |
| In−Br(2e) | 341.9(3) | | |
| In−Br(2f) | 345.6(3) | | |
| In−Br(3h) | 347.1(3) | | |
| In−Br(1c) | 350.2(3) | | |
| In−Br(3) | 357.5(3) | | |
| In−Br(1e) | 406.1(3) | | |
| Cr−Br(3) | 252.3(4) | Cr−Cr(c) | 376.3(5) |
| Cr−Br(2) | 255.3(4) | Cr−Cr(d) | 410.9(5) |
| Cr−Br(1) | 257.3(4) | Cr−Cr(a) | 412.1(5) |
| Cr−Br(1d) | 257.7(4) | Cr−Cr(d) | 412.1(5) |
| Cr−Br(2a) | 291.8(4) | | |
| Cr−Br(1c) | 310.9(4) | | |
| Br(1)−Br(1d) | 351.6(3) | Br(2)−Br(2c) | 377.6(3) |
| Br(1)−Br(2) | 362.1(3) | Br(2)−Br(2d) | 388.2(3) |
| Br(1)−Br(3c) | 366.4(3) | Br(2)−Br(3a) | 394.4(3) |
| Br(1)−Br(2b) | 377.9(3) | Br(2)−Br(2a) | 412.1(3) |
| Br(1)−Br(2a) | 384.8(3) | Br(2)−Br(3f) | 446.5(4) |
| Br(1)−Br(1c) | 396.0(3) | | |
| Br(1)−Br(3f) | 400.7(3) | Br(3)−Br(3a) | 412.1(3) |
| Br(1)−Br(3e) | 402.5(3) | Br(3)−Br(3b) | 412.1(3) |
| Br(1)−Br(3d) | 403.0(3) | | |
| Br(1)−Br(1a) | 412.1(3) | | |
| Br(1)−Br(1b) | 412.1(3) | | |

[a] Symmetry coding (including lattice translations): (a) $x - 1, y, z$; (b) $-x + 1, -y + 1, -z$; (c) $-x + 1, y + 1/2, -z + 1/2$; (d) $x - 1, y + 1/2, -z + 1/2$; (e) $x, -y + 1/2, z + 1/2$; (f) $x, -y + 1/2, z - 1/2$; (g) $x - 1, -y + 1/2, z + 1/2$.

and isotropic displacement parameters. Selected interatomic distances are given in Table 3.[9]

**2.2.2. Magnetic Structures of $InCrBr_3$ and $InFeBr_3$.** Powder samples of $InCrBr_3$ and $InFeBr_3$ (ca. 10 g) were sealed in vanadium containers ($\phi = 9$ mm, $V = 3.2$ mL), and neutron diffraction data sets (Diffractometer D1A of the ILL at Grenoble, France[10,11]) were obtained at temperatures of 280, 20, and 2 K.

For the data sets at 280 and 20 K, Rietveld refinements (FULLPROF[12]) were based on the X-ray single-crystal parameters for the two phases; both compounds did not show any crystallographic phase transitions at these temperatures. The $InFeBr_3$ sample, however, appeared to contain a large amount of $FeBr_2$ impurities (ca. 30%); its real origin is unknown but may be due to the decay of $InFeBr_3$. At 2 K both phases exhibited additional reflections that are due to magnetic ordering. Unfortunately, $FeBr_2$ exhibits antiferromagetic ordering, too. In the case of $InFeBr_3$ the magnetic reflections could be indexed using the crystallographic cell whereas for $InCrBr_3$ it had to be doubled along the short axis.

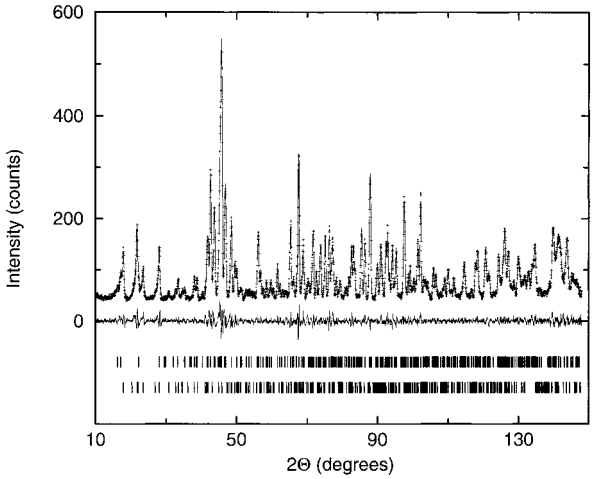


**Figure 1.** Rietveld refinement of the crystallographic and magnetic structures of $InCrBr_3$ at 2 K. Depicted are (from top to bottom) measured and fitted diffraction patterns, the difference between measured and calculated intensities, and the positions of the Bragg and magnetic reflections.

The magnetic structure of the chromium compound was finally solved by calculating a series of theoretical powder patterns for different models (LAZY PULVERIX[13]). The two possible spin alignments were first simulated using the scattering lengths of potassium and manganese which are of the same quantity but have different signs.[14] Thus, this starting model is almost equivalent with the scattering of two magnetic moments with opposite spin directions. The final Rietveld refinement of the complete data set, however, utilized the magnetic scattering factor for divalent chromium and was based on the only model which gave full agreement: the components of the magnetic vector were derived from the refinement.

The background of the $InCrBr_3$ data was at first manually corrected by linear interpolation and, in the last cycle, smoothed by linear, nonrecursive filtering (filter width 1% of the data points). The refinement itself is based on two different profile functions for crystallographic and magnetic phase respectively. There are 10 parameters for the peak shape (2 × pseudo-Voigt), 1 asymmetry parameter, 1 zero-point parameter, 1 parameter for preferred orientation (March−Dollase function), 1 overall scale parameter, 4 parameters for the lattice constants, 15 spatial atomic parameters, 3 isotropic displacement parameters, and 2 parameters for the magnetic moment. On the basis of the number of Bragg reflections, the refinement exhibits a 11-fold overdetermination. An overview of the refinement is given in Figure 1, while all numerical details are listed in Table 4.

The magnetic diffraction pattern of $InFeBr_3$ is so similar to the one of $KFeCl_3$ that the magnetic structure of the latter phase could be used as a start for the final Rietveld analysis.[15] It was performed on the complete data set using the magnetic scattering factor for divalent iron. Unfortunately, the strongest magnetic reflection at $2\Theta = 5.5°$ could not be measured with the D1A diffractometer because of the position of its beam stop; thus, a second measurement at 2 K was undertaken (Diffractometer TAS1 at the National Laboratory in Risø, Danmark). Since the resolution of the second data set is significantly lower, all structure parameters were first refined using the D1A data set. For the TAS1 data set, all D1A-refined positional and displacement parameters

(9) A list of the observed and calculated structure factors may be obtained from R.D.
(10) Hewat, A. W. *Nucl. Instrum. Methods* **1975**, *127*, 361.
(11) Hewat, A. W.; Bailey, I. *Nucl. Instrum. Methods* **1976**, *137*, 463.
(12) Rodriguez-Caravajal, R. *FULLPROF (Version 3.2)*; Laboratoire Léon Brillouin: January 1997.
(13) Yvon, K.; Jeitschko, W.; Parthé, E. *J. Appl. Crystallogr.* **1977**, *10*, 73.
(14) Sears, V. F. *Neutron News* **1992**, *3*, 26.
(15) Gurewitz, E.; Makovsky, J.; Shaked, H. *Phys. Rev. B* **1973**, *9*, 1071.

**Table 4.** Crystallographic and Magnetic Data for $InCrBr_3$ at 2 K

| | |
|---|---|
| formula | $InCrBr_3$ |
| lattice constants | $a = 408.46(1)$ pm, $b = 1490.45(3)$ pm, $c = 928.08(2)$ pm, $\beta = 93.977(1)°$ |
| magnetic unit cell | $2a, b, c$ |
| space group; Shubnikov group | $P2_1/c$ (no. 14); $P_{2a}2_1/c$ |
| absorption coefficient | 0.9057 $cm^{-1}$ |
| sample dimensions | vanadium container ($\phi = 0.9$ cm) |
| instrument; neutron wavelength | D1A (ILL Grenoble), $\lambda_N = 227.76$ pm |
| scan type, range, step, width | $2\Theta$, $10° \le 2\Theta \le 148.00°$, 0.05°, 6° |
| temperature | 2 K |
| no. of data points; Bragg and magnetic reflections | 2761; 358; 331 |
| absorption correction | cylindrical |
| magnetic structure solution | trial-and-error |
| structure refinement | Rietveld least-squares (FULLPROF) |
| $M_x, M_y, M_z$ | −3.50(9), 0, 3.10(6) |
| absolute value of $\vec{M}$ | 4.83(7) $\mu_B$ |
| profile function | pseudo-Voigt |
| $\eta$, $x$ mixing parameters | 0.30(3), −0.0022(4) (cryst.) 1.6(1), −0.025(4) (magn.) |
| $u$, $v$, $w$ half-width parameters | 0.155(4), −0.34(1), 0.326(7) (cryst.) 0.3(1), −0.6(1), 0.36(3) (magn.) |
| asymmetry parameter | 0.031(4) (magn.) |
| preferred orientation function | March−Dollase, $G = 0.942(2)$ |
| no. of variables, constraints, restraints | 39, 10, 0 |
| zero point | −0.392(2) |
| $R_p$; $R_{wp}$ | 0.047; 0.060 |
| $R_{Bragg}$; $R_{mag}$; goodness of fit | 0.027; 0.057; 0.54 |

were fixed, and only the lattice parameters, magnetic moments, and the overall parameters (profile function, zero point, scale factor) were refined.

As in the case of $InCrBr_3$, the background of the $InFeBr_3$ data was at first manually corrected by linear interpolation; in the last refinement cycle it was linearly smoothed by Fourier filtering (filter width 1% of the data points). The magnetic and crystallographic results are based on (D1A data set) 5 parameters for the profile function (pseudo-Voigt), 1 zero-point parameter, 2 parameters ($InFeBr_3$ and $FeBr_2$) for preferred orientation (March−Dollase function), 2 overall scale parameters, 3 parameters for the lattice constants of $InFeBr_3$, 2 parameters for the lattice constants of $FeBr_2$, 10 spatial atomic parameters for $InFeBr_3$, 1 spatial atomic parameter for $FeBr_2$, 3 isotropic displacement parameters (coupled for both phases), and 1 parameter each for the magnetic moments. To refine the TAS1 data set, we used 3 parameters for the peak shape (Gauss), 1 zero-point parameter, 1 parameter for the preferred orientation of $FeBr_2$ (March−Dollase function), 2 overall scale parameters, 3 parameters for the lattice constants of $InFeBr_3$, 2 parameters for the lattice constants of $FeBr_2$, and 1 parameter each for the magnetic moments. An overview of the two refinements is given in Figure 2, whereas all numerical details can be found in Table 5.

**2.3. Magnetic Susceptibility Measurement.** A crystalline sample of 177.3 mg was subjected to a susceptibility measurement by use of a Quantum Design MPMS 5.5 Squid susceptometer within a temperature range of 2−320 K at a field of 1 T. The influence of the electron core shells on the molar susceptibility was corrected using tabulated diamagnetic values for the different ions.[16] The value of $In^+$ ($-23 \times 10^{-6}$ emu/mol) was taken from a previous investigation.[17]

**2.4. Band Structure Calculations.** Ab initio electronic structure calculations were performed using LMTO (Linear Muffin-Tin Orbital[18]) and density-functional theory, the latter parametrized according to von Barth and Hedin.[19] All diagonalization and integration tasks of the spin-polarized scalar-relativistic $k$ space Hamiltonian were performed with the help of an improved tetrahedron method using 78 inequivalent $k$ points and 576 different tetrahedra. The basis set of short-ranged[20] atom-centered TB-LMTOs contained s−f valence functions for In and s−d valence functions for all other atoms. Additionally, another 24 "empty spheres" per cell were incorporated in order to increase variational freedom and improve packing.

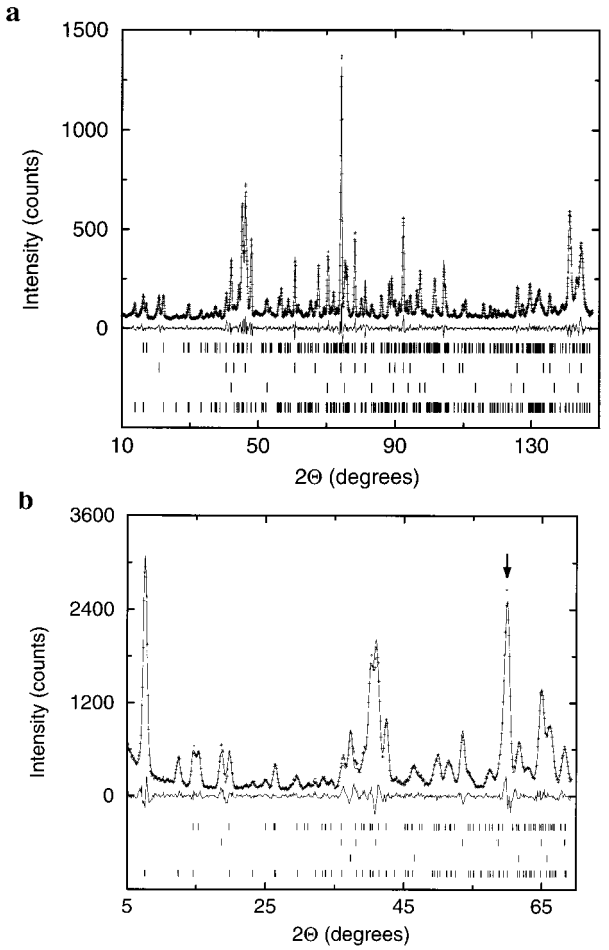


**Figure 2.** (a) Rietveld refinement of the crystallographic and magnetic structures of $InFeBr_3$ and $FeBr_2$ at 2 K (D1A). Depicted are (from top to bottom) measured and fitted diffraction patterns, the difference between measured and calculated intensities, the positions of the Bragg reflections of $InFeBr_3$ and $FeBr_2$, and those of the magnetic reflections of $FeBr_2$ and $InFeBr_3$. (b) Rietveld refinement of the crystallographic and magnetic structure of $InFeBr_3$ and $FeBr_2$ at 2 K (TAS1). Depicted are (from top to bottom) measured and fitted diffraction patterns, the difference between measured and calculated intensities, the positions of the Bragg reflections of $InFeBr_3$ and $FeBr_2$, and those of the magnetic reflections of $FeBr_2$ and $InFeBr_3$. At about $2\Theta = 59°$ there is a reflection (arrow) of the aluminum container that was fitted in the profile matching mode.

The structure was iterated by use of the atomic-spheres approximation (ASA), employing muffin-tin spheres enlarged to overlapping and volume-filling spheres, including a combined correction term. The bonding within the solid state was analyzed using the COHP method,[21] a first principles method equivalent of the COOP technique, providing interatomic bonding information. The program used was TB-LMTO 4.7C,[22] run on an IBM AIX 43P-133 workstation.

## Results and Discussion

**3.1. Description of the Crystal Structure.** The crystal structure of $InCrBr_3$ ($P2_1/c$) is closely related to the one of $InFeBr_3$ and $InMnBr_3$ ($Pnma$),[23] and $InCrBr_3$ crystallizes in a distorted variant of the $NH_4CdCl_3$ structure type, a projection

(16) Selwood, P. W. *Magnetochemistry*, 2nd ed.; Interscience Publishers: New York, 1956.
(17) Dronskowski, R. Ph.D. Thesis, Universität Stuttgart (FRG), 1990.
(18) Andersen, O. K. *Phys. Rev. B* **1975**, *12*, 3060.
(19) von Barth, U.; Hedin, L. *J. Phys. C* **1972**, *5*, 1629.
(20) Andersen, O. K.; Jepsen, O. *Phys. Rev. Lett.* **1984**, *53*, 2571.
(21) Dronskowski, R; Blöchl, P. E. *J. Phys. Chem.* **1994**, *97*, 8617.
(22) Krier, G.; Jepsen, O.; Burkhardt, A.; Andersen, O. K. Program TB-LMTO 4.7; Max-Planck-Institut für Festkörperforschung, Heisenbergstr. 1, D-70 569 Stuttgart (FRG).
(23) Dronskowski, R. *Inorg. Chem.* **1994**, *33*, 5927.

**Table 5.** Crystallographic and Magnetic Data for $InFeBr_3$ at 2 K

| | | |
|---|---|---|
| formula; formula units | $InFeBr_3$; 4 | |
| lattice constants | $a = 925.62(3)$ pm, $b = 393.06(1)$ pm, $c = 1498.56(5)$ pm | $a = 923.0(3)$ pm, $b = 392.71(8)$ pm, $c = 1496.0(4)$ pm |
| magnetic unit cell | *a*, *b*, *c* | |
| space group; Shubnikov group | *Pnma* (no. 62); *Pnma* | |
| absorption coefficient[a] | 0.3372 $cm^{-1}$ | |
| sample dimensions | vanadium container ($\phi = 0.9$ cm) | aluminum container ($\phi = 0.9$ cm) |
| instrument; wavelength | D1A (Grenoble); $\lambda_N = 227.76$ pm | TAS1 (Risø); $\lambda_N = 201.941$ pm |
| scan type, range, step, width | $2\Theta$; $7° \le 2\Theta \le 148.00°$, 0.05°, 6° | $2\Theta$; $4° \le 2\Theta \le 69.29°$, 0.10°, 0.10° |
| temperature | 2 K | |
| no. of data points; Bragg and magnetic reflections | 2796; 212; 320 | 655; 68; 91 |
| absorption correction | cylindrical | |
| magnetic structure solution | structure of $KFeCl_3$ | |
| structure refinement | Rietveld least-squares method (FULLPROF) | |
| direction of $\vec{M}$ | [010] | |
| absolute value of $\vec{M}$ | 4.95(6) $\mu_B$ | 5.06(4) $\mu_B$ |
| profile function | pseudo-Voigt | Gauss |
| $\eta$, *x* mixing parameters | 0.61(3), −0.0035(3) | − |
| *u*, *v*, *w* half-width parameters | 0.244(4), −0.50(1), 0.396(7) | 0.9(2), −0.12(16), 0.49(2) |
| preferred orientation | March−Dollase, $G = 0.907(3)$ | none |
| no. of variables, constraints, restraints | 31, 7, 0 | 14, 11, 0 |
| zero point | −0.384(2) | −0.194(4) |
| $R_p$; $R_{wp}$ | 0.055; 0.074 | 0.062; 0.084 |
| $R_{Bragg}$; $R_{mag}$; goodness of fit | 0.032; 0.058; 0.79 | 0.034; 0.039; 1.7 |

[a] Calculated from $\mu(InFeBr_3) = 0.4787$ $cm^{-1}$ and $\mu(FeBr_2) = 0.1183$ $cm^{-1}$ using a mass ratio of 3:2 for $InFeBr_3$:$FeBr_2$.

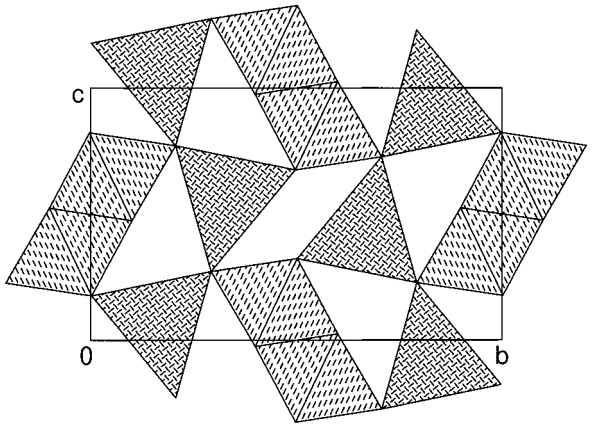


**Figure 3.** Polyhedral projection of the $InCrBr_3$ crystal structure along the *a* axis. The univalent indium cations are within trigonal bromine prisms, whereas the divalent chromium cations are located in vertex-sharing bromine octahedra (with dashed line pattern).

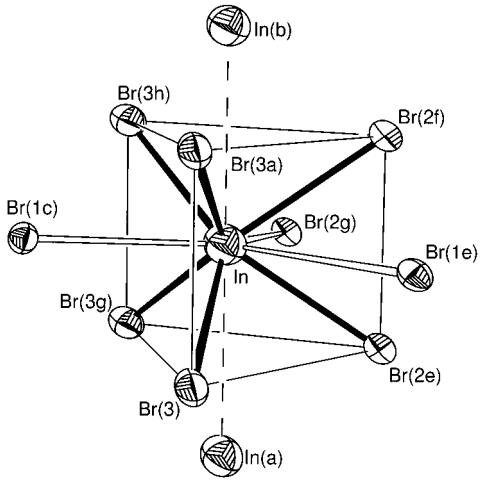


**Figure 4.** Perspective view of the $In^+$ coordination by $Br^-$ anions in $InCrBr_3$. The thermal ellipsoids enclose 70% of the electrons' spatial probability. The $In^+-Br^-$ bonds are given as solid ($Br^-$ inside the trigonal prism) and open (face-capping $Br^-$) lines, whereas the shortest $In^+-In^+$ contacts are drawn with broken lines. The edges of the polyhedron are emphasized by thin lines.

of which is given in Figure 3. Indeed, the space group $P2_1/c$ is a maximum *translationengleiche* subgroup of *Pnma* with index 2.[24]

The $Cr^{2+}$ ions are coordinated by six bromine anions which form a distorted octahedron. While four $Br^-$ ions are found at an average distance of 256 pm, the two remaining ones are 291 and 311 pm away. The shorter distances are in good agreement with the short $Cr^{2+}-Br^-$ bond length in $CrBr_2$ and also the arithmetic mean (301.4 pm) of the longer ones is comparable with the corresponding distance (299.8 pm) in $CrBr_2$.[25] We note that the $M^{2+}-Br^-$ bond length spectra of the isotypic phases containing Fe, Mn, and Cd are much narrower, with average distances of 265 ± 11 pm ($InFeBr_3$), 271 ± 10 pm ($InMnBr_3$), and 278 ± 12 pm ($InCdBr_3$). Taking into account that $Cr^{2+}$ is a $d^4$ system and presupposing a high-spin complex, then the $Cr^{2+}-Br^-$ bond lengths are characteristic of a Jahn−Teller distortion. We come back to this aspect in the Magnetic Properties section. The $CrBr_6^{4-}$ octahedron shares vertices with four other octahedra, resulting in a double chain of octahedra running parallel to the *a* axis.

Univalent indium atoms are located in strongly distorted trigonal prisms with bond lengths covering a range of 322−357 pm. Such a polyhedron is shown in Figure 4 as a thermal ellipsoid plot. Three additional $Br^-$ ions overcap the rectangular faces of the prism with a wide distance spectrum of 335−406 pm such that there results an empirical bond order sum for indium of 1.10.[3] The prism's top and bottom triangular faces are capped by indium atoms from the neighboring cell, giving $In^+-In^+$ contacts of about 412 pm. Among the face-capping ligands there is one which is about 21% further away from the central indium atom than the other two. From a classical, more electrostatic point of view one might believe that this finding is due to a so-called direct electron "lone-pair" effect. However, ab initio calculations for $InFeBr_3$, $InMnBr_3$, and $InCdBr_3$ showed that the inequality in the interatomic distances actually arises from a pure packing reason.[23,26]

(24) Bärnighausen, H. *Comm. Math. Chem.* **1980**, *9*, 139.
(25) Tracy, J. W.; Gregory, N. W.; Lingafelter, E. C. *Acta Crystallogr.* **1962**, *15*, 672.

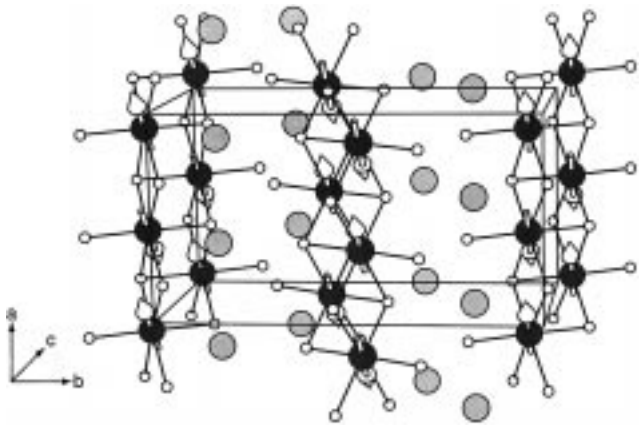


**Figure 5.** Perspective view of the magnetic structure of $InCrBr_3$ with the magnetic unit cell, showing the $Cr^{2+}$ cations as dark shaded spheres, $In^+$ cations as light shaded spheres, and $Br^-$ as small circles.

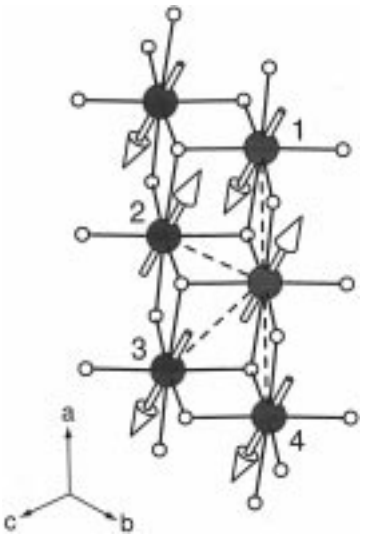


**Figure 6.** Double chain of octahedra in $InCrBr_3$ along the *a* axis. The chromium atoms are depicted as dark shaded spheres, the bromine atoms as small open circles, and the chromium−bromine bonds as rods. The four nearest neighbors of one chromium atom are enumerated.

There is one open question: Why does $InCrBr_3$ adopt a monoclinic structure, unlike orthorhombic $InFeBr_3$, $InMnBr_3$, and $InCdBr_3$? If one recalculates all interatomic distances and angles using the monoclinic symmetry elements and the monoclinic angle $\beta$ set to 90°, there seems to be no drastic change for any of the atoms. We come back to this question in the Electronic Structure section.

**3.2. Description of the Magnetic Structures. 3.2.1. The Magnetic Structure of $InCrBr_3$.** The magnetic unit cell (Figure 5) of $InCrBr_3$ is twice as large as the crystallographic one and can be obtained by doubling the short *a* axis. The chromium ions of oxidation state +2 have magnetic moments with a value of 4.83(7) $\mu_B$ (using $\mu = 2\sqrt{S(S+1)}$) pointing in the $[\bar{1}01]$ direction. The magnetic ordering takes place in the double chain of octahedra, and there are parallel as well as antiparallel alignments. Each of the chromium atoms has four nearest chromium neighbors within a double chain, two in the [100] direction (atoms 1 and 4 in Figure 6, hence within one "single" octahedron string) and another two in the neighboring chain (atoms 2 and 3). The distances in the direction of the *a* axis (409 pm) are identical with the crystallographic lattice parameter. Toward the neighboring string, there are two different distances: a short one (367 pm, atom 2) and a long one (408 pm, atom 3). Parallel spin alignment between different $Cr^{2+}$ is found for the short distance and antiparallel alignment for the long distance. In the direction of the *a* axis, there is antiparallel coupling throughout. This yields to pairs of parallel spins which interact antiferromagnetically along the short *a* axis.

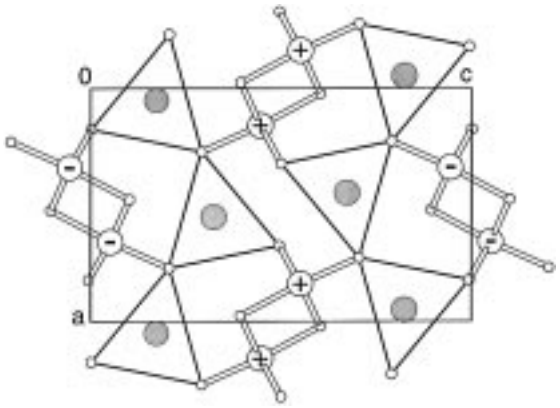


**Figure 7.** View of the magnetic structure of $InFeBr_3$ along the *b* axis. The two spin directions of the Fe atoms are depicted in hatching (+ and −). The bromine atoms appear as small spheres and the indium atoms as light shaded spheres.

Neutron diffraction cannot clarify whether those spins along the long distance do couple indeed ferromagnetically or whether the parallelism is forced by the whole spin arrangement. Nevertheless, a distance of 367 pm rules out any direct spin interactions. On the contrary, a hypothetical ferromagnetism must be mediated via the bridging bromine atoms, and the same (super exchange) has to be stated for the antiparallel spins.

To describe the symmetry of this phase's magnetic structure, one can refer to the Shubnikov subgroups of $P2_1/c$. The spin arrangement within the half of the magnetic cell (≡crystallographic cell) can be described by the symmetry elements of space group $P2_1/c$. Since the magnetic unit cell is obtained by doubling the crystallographic one along the *a* axis, the Shubnikov group has to be $P_{2a}2_1/c$.

**3.2.2. The Magnetic Structure of $InFeBr_3$.** $InFeBr_3$ has the same magnetic structure as the isotypic phase $KFeCl_3$.[15] All spins within the double chains of octahedra couple ferromagnetically. The ordering between the double chains is antiferromagnetic, giving layers of double chains with equal spin alignment in the [100] direction; Figure 7 shows the magnetic structure of $InFeBr_3$. The magnetic moment coincides with the *b* axis and amounts to 4.95(6) $\mu_B$ (D1A) or 5.06(4) $\mu_B$ (TAS1), reflecting the expected four unpaired electrons for $Fe^{2+}$ ($\mu = 2\sqrt{S(S+1)}$).

The Shubnikov group has been determined from a list of different magnetic configurations for the Wyckoff position in space group *Pnma* (Table 6).[27] The magnetic reflections of $InFeBr_3$ follow the reflection conditions $k + l$ uneven for (0*kl*) and *h* uneven for (*hk*0). Thus, configuration C (Table 6) is valid; since the magnetic moment coincides with the *b* axis, the Shubnikov group is *Pnma*.

**3.3. Magnetic Properties.** Figure 8 shows plots of molar susceptibility and reciprocal molar susceptibility as a function of temperature for $InCrBr_3$. It is evident that $InCrBr_3$ exhibits Curie−Weiss paramagnetism and is subject to antiferromagnetic ordering below a Néel temperature $\Theta_N$ of 12 K.

(26) Dronskowski, R. *J. Solid State Chem.* **1995**, *116*, 45.

(27) Gurewitz, E.; Shaked, H. *Acta Crystallogr. A* **1972**, *28*, 280.

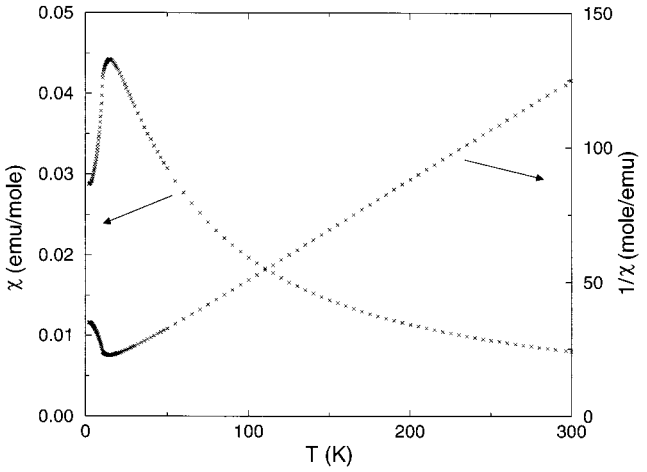


**Figure 8.** Molar susceptibility and reciprocal molar susceptibility as a function of the temperature for $InCrBr_3$ ($H = 1$ T).

**Table 6.** Classification of the Magnetic Configurations for the Wyckoff Position 4*c* in *Pnma*

| | reflection condition | | magnetic groups | | |
|---|---|---|---|---|---|
| configuration | (0*kl*) | (*hk*0) | $\vec{M}\|\|x$ | $\vec{M}\|\|y$ | $\vec{M}\|\|z$ |
| G | $k+l=2n$ | $h=2n+1$ | $mn'a$ | $n'ma$ | $n'm'a'$ |
| A | $k+l=2n+1$ | $h=2n$ | $n'm'a'$ | $nma'$ | $nm'a$ |
| C | $k+l=2n+1$ | $h=2n+1$ | $n'm'a$ | $nma$ | $nm'a'$ |
| F | $k+l=2n$ | $h=2n$ | $nm'a'$ | $n'ma'$ | $n'm'a$ |

A linear fit of the data between 50 and 320 K results in a Curie temperature Θ of −19.4 K and an effective moment $\mu_{eff}$ of 4.80 $\mu_B$. This is in good agreement with the neutron data and with the theoretical spin-only value for a $Cr^{2+}$ ion with $S = {}^4/_2$ (4.90 $\mu_B$ for $\mu = 2\sqrt{S(S+1)}$) and previous experimental data (4.80−5.00 $\mu_B$).[28]

**3.4. Electronic Structure.** In Figure 9a we show the total and local (In) density of states (DOS) for $InCrBr_3$, calculated using the LMTO method in the spin-polarized mode. The indium contributions fall into two different parts. In the occupied energy region below the Fermi level there are large contributions of the Br centered 4p orbitals; the In 5s orbitals are also mixed into this range. The virtual indium 5p levels are found above −2.2 eV. The very low lying bromine 4s bands do not appear in this energy window.

Now we will focus on the local DOS for chromium (Figure 9b) which originates from the Cr 3d levels; their splitting can be understood using ligand field theory. Within an octahedral ligand field the five d orbitals split into two different sets with $t_{2g}$ and $e_g$ symmetry (Figure 10). The magnetic measurement revealed four unpaired electrons on each $Cr^{2+}$ cation, corresponding to a $d^4$ high spin situation. Thus, each of the three orbitals of the $t_{2g}$ set must be filled with one electron while the fourth one resides in the $e_g$ set. Whenever a degenerate HOMO is incompletely filled, one can expect a Jahn−Teller distortion to happen: the axial and equatorial bond lengths become different. This situation is indeed found in $InCrBr_3$: two Cr−Br distances (top and bottom) are significantly larger than the other four (Table 3). The additional 20 pm difference between the two long bonds is probably due to packing reasons.

Figure 10 also shows the relative energies of the d orbitals in an elongated octahedral ligand field. The $d_{x^2-y^2}$ orbital, directed to the equatorial ligands, becomes strongly destablized. The $d_{z^2}$ orbital, on the other hand, gets lowered in energy.

(28) Weiss, A.; Witte, H. *Magnetochemie*, 1st ed.; Verlag Chemie: Weinheim, 1973.

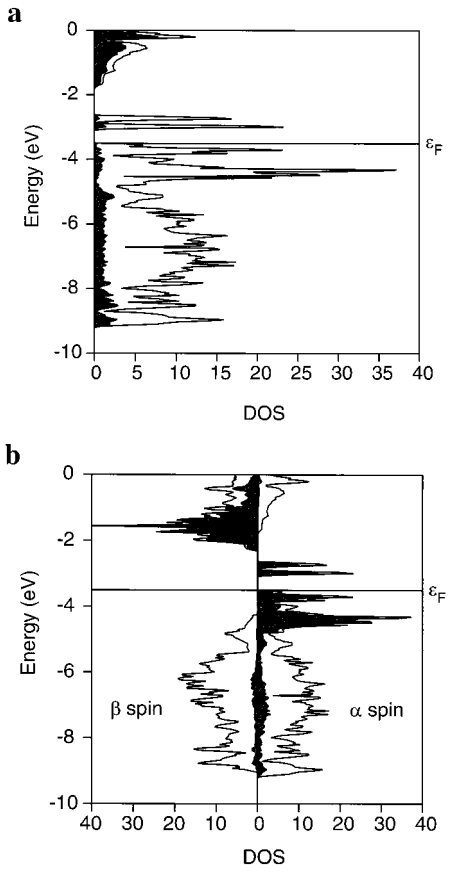


**Figure 9.** TB-LMTO-ASA density of states (DOS) of $InCrBr_3$. (a) Indium contributions have been shaded; (b) emphasizing the chromium contributions (spin-polarized).

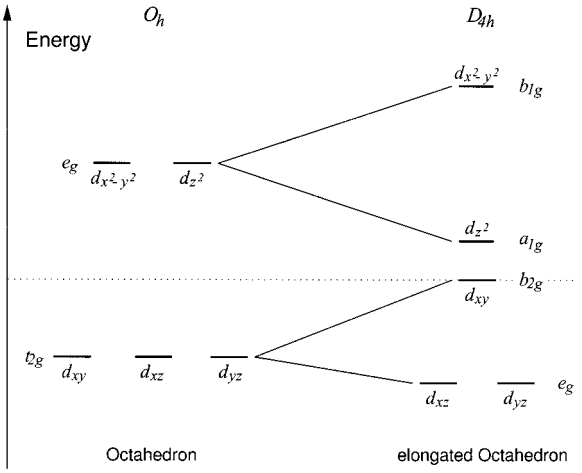


**Figure 10.** Diagram of the relative energies of d orbitals for a regular octahedral (left) and a distorted octahedral (right) ligand field. The crucial point of energy is given as a dashed line.

The projected DOS for chromium shows contributions of the d bands between −4.9 eV and the Fermi level. This region contains the four d orbitals $d_{xy}$, $d_{xz}$, $d_{yz}$, and $d_{z^2}$, each of which is filled with one electron. Around −3 eV there is a double peak which can be assigned to the empty $d_{x^2-y^2}$ band (compare with Figure 10). Indeed, the ratio between the area of the empty double peak and the occupied d region below the Fermi level is the expected value of 1:4. The additional splitting of the unfilled $d_{x^2-y^2}$ bands can be explained by the interaction of two chromium atoms via the bridging bromine atoms, supported by the mixing in of bromine levels into this region. Above −2.3

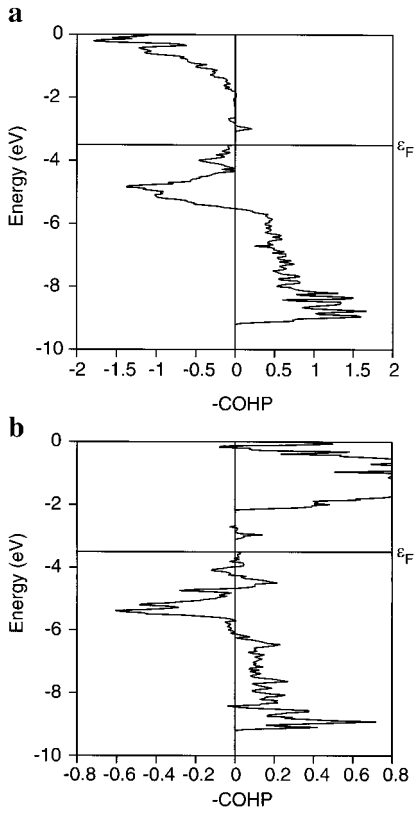


**Figure 11.** TB-LMTO-ASA COHP for the (a) nine shortest $In^+-Br^-$ contacts of $InCrBr_3$ and (b) the two shortest $In^+-In^+$ contacts of $InCrBr_3$.

eV there are also strong d contributions; these are the empty d orbitals with the opposite spin direction ($\beta$ spin).

To focus on the $In^+-Br^-$ bonding, the corresponding COHP for the nine nearest $In^+-Br^-$ contacts is presented in Figure 11a. The situation is well-known from interactions between monovalent indium and bromine cations.[23] Below $-5.5$ eV, in the region of the bromine 4p block and up to the lower margin of the indium 5s band, there are strong bonding interactions. The highest occupied levels, however, are of antibonding nature due to out-of-phase In 5s−Br 4p interactions. This leads to an integrated COHP value of $-2.06$ eV for the overall $In^+-Br^-$ bonding.

**Table 7.** ICOHP Values (eV) in $InCrBr_3$ for the Monoclinic and Pseudo-Orthorhombic Crystal System

| | −ICOHP | |
|---|---|---|
| bonds | monoclinic | pseudo-orthorhombic |
| In−Br | 2.06 | 2.20 |
| In−In | 0.09 | 0.09 |
| Cr−Br | 8.00 | 7.60 |

A COHP plot for the shortest indium−indium contacts is depicted in Figure 11b. Generally there are very weak bonding interactions, giving an integrated COHP of only $-0.09$ eV. As expected, the interactions between chromium and bromine (COHP not shown) are strongly bonding: the integrated COHP is $-8.0$ eV.

Upon changing to a hypothetical orthorhombic cell ($\beta = 90°$), the total energy increases by more than 100 kJ/mol. In Table 7 the ICOHP values for the monoclinic and the hypothetical orthorhombic cell are compared with each other. It is clear that the $In^+-Br^-$ interactions are somewhat weakened for an orthorhombic system (about 7%) but the $Cr^{2+}-Br^-$ bonds are evidently stronger in the case of the real monoclinic structure. Thus, the Jahn−Teller distortion does not only change the local symmetry around $Cr^{2+}$ but it also proves to be the structure-determining element (crystal class) in $InCrBr_3$.

**Acknowledgment.** It is a pleasure to thank Dr. Alan W. Hewat for competent help in the neutron data collection as well as Mrs. Eva Brücher and Dr. Reinhard Kremer for the susceptibility measurements. We thank Dr. Paul Müller for sharing his expertise in magnetic Rietveld refinements. The additional financial support by a Kekulé scholarship of the Fonds der Chemischen Industrie (Frankfurt) provided to M.S. is gratefully acknowledged.

**Supporting Information Available:** Tables of crystallographic and structure refinement data and anisotropic displacement parameters. This material is available free of charge via the Internet at http://pubs.acs.org.

IC981383T